



Unsteady natural convection of nano-encapsulated phase change materials (NEPCMs) inside a random porous medium considering local thermal non-equilibrium condition

Mehdi Ghalambaz^{a,b}, S. A. M. Mehryan^c, Mohammad Vaezi^d, Iman Zahmatkesh^e, Ahmad Hajjar^f, Obai Younis^{g,h} and Mohammad Ghalambaz^{i,j}

^aInstitute of Research and Development, Duy Tan University, Da Nang, Vietnam; ^bFaculty of Electrical – Electronic Engineering, Duy Tan University, Da Nang, Vietnam; ^cYoung Researchers and Elite Club, Yasooj Branch, Islamic Azad University, Yasooj, Iran; ^dFaculty of Mechanical Engineering, K. N. Toosi University of Technology, Tehran, Iran; ^eDepartment of Mechanical Engineering, Mashhad Branch, Islamic Azad University, Mashhad, Iran; ^fECAM Lyon, LabECAM, Université de Lyon, Lyon, France; ^gDepartment of Mechanical Engineering, College of Engineering at Wadi Addwaser, Prince Sattam Bin Abdulaziz University, Wadi Addwaser, Saudi Arabia; ^hDepartment of Mechanical Engineering, Faculty of Engineering, University of Khartoum, Khartoum, Sudan; ⁱMetamaterials for Mechanical, Biomechanical and Multiphysical Applications Research Group, Ton Duc Thang University, Ho Chi Minh City, Vietnam; ^jFaculty of Applied Sciences, Ton Duc Thang University, Ho Chi Minh City, Vietnam

ABSTRACT

A local thermal non-equilibrium analysis is undertaken to simulate unsteady free convective heat transfer inside a square enclosure filled with a random porous medium. There is a time-varying temperature profile at the hot wall. The fluid is a suspension comprising nano-encapsulated phase change materials (NEPCM) particles dispersed in water while aluminum foam, copper foam, or glass balls are considered for the solid matrix. It is found that when the hot wall temperature reaches its minimum value during one oscillation period, most of the cavity is occupied by the NEPCM particles in the solidious phase. For the metallic foams, the heat transfer of the medium is substantially higher than the NEPCM particles. Meanwhile, the Nusselt number of the glass balls is much lower than the suspension. A rise in the dimensionless frequency or amplitude of the temperature profile as well as approaching the dimensionless fusion temperature to 0.5 elevates Nusselt number of the suspension. However, no general conclusion can be drawn for their consequences on the heat transfer in the solid matrix. Among the current alterable parameters, only the contributions of the non-dimensional interface heat transfer coefficient and the non-dimensional amplitude of the temperature profile are found significant.

ARTICLE HISTORY

Received 22 February 2022
Accepted 6 June 2022

KEYWORDS

Unsteady heat transfer;
Porous media; Cavity; Local
thermal non-equilibrium
(LTNE) model;
Nano-encapsulated phase
change material (NEPCM)

1. Introduction

The significantly growing demands for energy in the last few decades have increased the efforts to seek alternative energy resources and to improve energy storage systems. Thermal energy storage using Phase Change Materials (PCM) is a latent heat based storage

method that has been shown to be effective in a number of engineering applications, including the cooling of electronic devices [1], the thermal comfort in buildings [2], and domestic air-conditioning systems [3] among others.

The significance of the PCM lies in their ability to absorb and release energy if they melt or solidify at temperatures similar to their fusion temperature when they come into contact with a hotter environment. Consequently, the PCM provides a substantial advantage due to their remarkable latent heat for a relatively little difference in temperatures. Nonetheless, the low thermal conductivity of the PCM presents a significant drawback as it limits their efficiency in terms of heat transfer. In this context, a variety of techniques have been used to increase the thermal conductivity of the PCMs [4]. Among these techniques, a widely-used method consists of dispersing nanoparticles in the PCM, leading to the so-called Nano-Enhanced PCM [5].

In systems where the discrepancy in the thermal expansion coefficient between the various materials may lead to a substantial temperature gradient, such as computer chips or laser alignment devices, the encapsulation of the PCM can be effectively used to improve the temperature control. Encapsulating consists of using shell–core structured capsules where the core is made of PCM. Based on the capsule size, a distinction is often made between nano-encapsulated and micro-encapsulated PCM [6]. The term nano-encapsulated PCM (equally abbreviated as NEPCM) is normally used when the characteristic size of the capsule is below 100 nm. NEPCM suspensions are considered a class of nanofluids. Another technique is based on metallic foams, which, due to their low density to surface area ratio, have been widely used as an enhancement of the PCM thermal conductivity. Such porous metallic media in the system present different aspects that can greatly affect the hydrodynamic and thermal behaviors.

In this context, it has been the topic of current research to examine free convective flows within enclosed porous media systems. Various types of enclosures have been considered, such as cavities partially filled with porous media [7,8], filled with several layers [9,10], porous fins [11], inclined cavities [12], wavy cavities [13,14], and enclosures undergoing non-uniform heating [15].

Another way of improving the thermal conductivity of suspensions is to use nanoparticles as nano additives, as investigated in [16–18]. Thus, the heat transfer of nanofluids in enclosures filled with a porous media has been considered to cover different aspects, including the effects of internal heat generation [19,20], local thermal non-equilibrium (LTNE) [21], the nanoparticles shape [22], the enclosure inclination and the presence of partial porous layers [23,24]. The thermal convection of PCM in enclosures with the porous medium has also been investigated. Most of the previous works on this topic dealt with the presence of metallic foams as thermal conductivity enhancement [25–27].

As a new approach, the PCMs can be encapsulated in nanoshells to form Nano-Encapsulated Phase Change Material (NEPCM) particles. Then, NEPCM particles are suspended in a liquid to synthesize a NEPCM-suspension. Thus, the heat transfer of NEPCMs and their thermal energy storage are new topics that demand further investigation.

The convective flow of NEPCM suspensions has been studied extensively, with a particular emphasis being placed on forced convection of the NEPCM suspensions. The research group of Ho et al. conducted a series of studies on the heat transfer of encapsulated PCMs and suspensions in packed enclosures [28,29], forced convection in circular tubes [30] and

mini/micro channels [31,32] to compare the thermal and flow parameters of pure water to those of alumina nanoparticle suspensions and PCM capsules, which they found to be significantly different. They discovered that a range of factors, including the location of the heat source and the rate of the flow, influenced the rate of heat transfer.

Seyf et al. [33] carried out a computational investigation into the enhancement of heat transfer by NEPCM in microtubes. They came to the conclusion that, while using NEPCM with a high fraction resulted in a significant improvement in fluid cooling power, the pressure drop in the microtube was enhanced. In another study, Seyf et al. [34] addressed the heat transfer and flow past an unconfined cylinder and discovered that employing a NEPCM slurry significantly boosted heat transfer when compared to using a base fluid and that this effect increased with increasing NEPCM volume %. For example, in their study, Eisapour et al. [35] used a suspension of nano-PCMs to improve the thermal performance of a photovoltaic/thermal system. They discovered that employing the nano-PCM slurry improved both the energy and exergy efficiency of the system.

There has been insufficient attention paid to the natural convection caused by the suspension of NEPCM. Using numerical simulations, Ghalambaz and colleagues [36] examined the free convection of NEPCM inside a square enclosure with isothermal side walls and insulated horizontal walls. They came to the conclusion that the temperature of the PCM core fusion has a significant impact on the involvement of the NEPCM in the total heat transfer in the enclosure. For the hot wall temperature, Hajjar et al. [37] extended this analysis to include time-periodic conditions for the hot wall temperature and discovered that the PCM core fusion temperature, as well as the NEPCM fraction, are critical parameters affecting heat transmission in the enclosure. Alsedais and Aly [38] investigated the mixed convection heat transfer of NEPCM suspensions in an asteroid-shaped cavity in the presence of an oscillating baffle. The baffle undergoes a sin shape oscillation. The outcomes show Stefan and fusion parameters are two important contributing factors in enhancing phase change heat transfer.

Free convection of NEPCM in the presence of a porous media, on the other hand, has gotten less attention than it deserves. Recently, Zehba and Aly [39] examined the natural convection of NEPCM suspensions in a rotating cylinder cavity. They concluded a fusion-temperature controls the intensity and location of a phase change zone. Moreover, Ghalambaz et al. [40] examined the steady-state natural convection heat transfer of NEPCM in an enclosure subject to temperature differences at sidewalls. The enclosure was loaded with a porous media as the temperature of the side walls was constant. The NEPCM particles moved with the natural convection flow and contributed to the heat transfer in the form of sensible heat and latent heat. Their findings indicated that the presence of 5% NEPCM particles augmented the heat transfer rate by 47% when the porous media thermal conductivity was poor. Despite the fact that the NEPCM particles contributed to the heat transfer mechanism in [40], the nature of the flow and heat transfer were both steady state in nature. The influence of latent heat from NEPCMs on transient heat transfer applications, on the other hand, is not well understood.

Thus, following the steady-state investigations of [36,40], The present research intends to examine the transient heat transfer characteristics of a NEPCM in an enclosure loaded with a porous media under LTNE conditions for the first time. Different porous media are considered to encounter effects of the thermos-physical properties of the medium on the heat transfer performance of the NEPCM and the solid matrix inside the cavity.

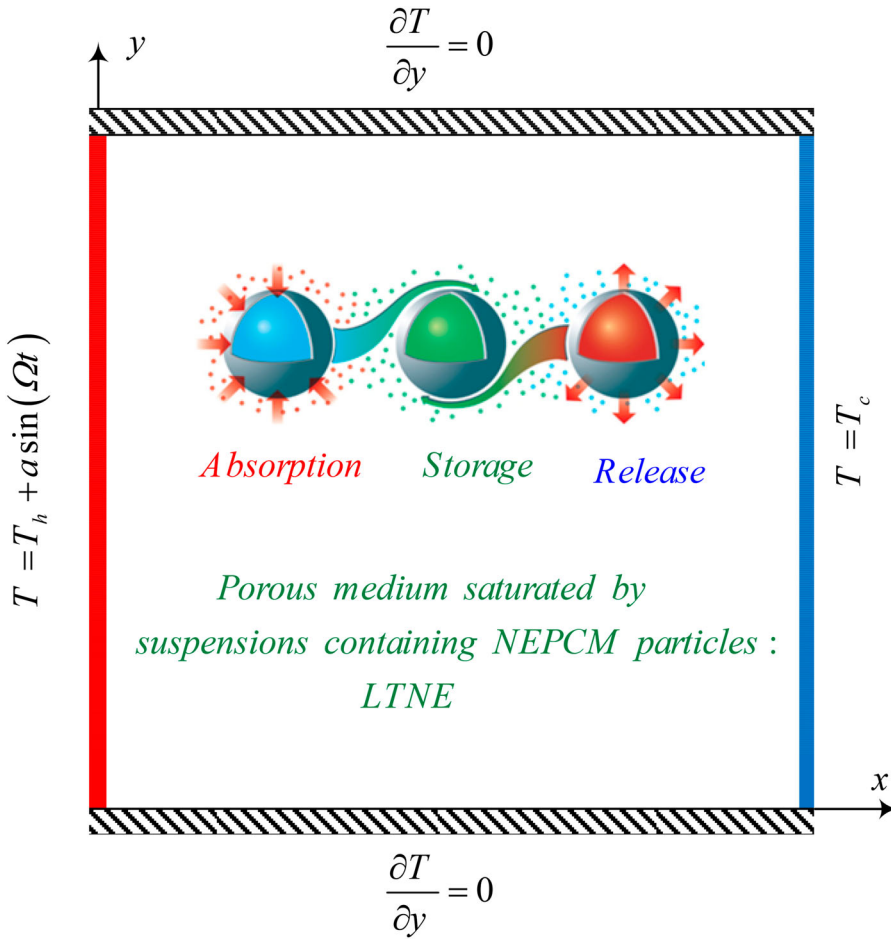


Figure 1. Schematic view of the geometry and model.

2. Problem formulation

The geometrical model of the considered cavity is illustrated in Figure 1. The cavity is square having the characteristic length of L , and filled with a porous medium. Initially, a steady-state is established, and then, a higher time-varying temperature, with an average T_h , is applied to the left wall. The right side of the cavity acts as a cold surface and has a lower temperature T_c . The other walls are adiabatic. A NEPCM suspension with water as the base fluid has been considered a working fluid. Temperature differences exist between the suspension and the solid matrix on a localized scale, as seen in Figure 1. The microscopic heat transfer between the components of the porous media is responsible for establishing the energy balance between them. No temperature nor hydrodynamic slips exist between the host fluid and the dispersed NEPCM particles. The NEPCM particles are made up of a phase change material encased in a shell. The nonadecane core and polyurethane (PU) shell were used in the construction of the core and shell, respectively.

Table 1. Thermophysical parameters of solid matrices and the suspension's elements.

Materials	k (W/m.K)	ρ (Kg/m ³)	C_p (J/Kg.K)	β (K ⁻¹)	μ (kg/m. s)
Host fluid	0.613	997.1	4179	21.0×10^{-5}	8.9×10^{-4}
Glass balls	1.05	2700	840	0.90×10^{-5}	–
Aluminum foam	205	2700	897	2.22×10^{-5}	–
Copper foam	400	8933	385	1.67×10^{-5}	–
PU		786	1317.7		–
Nonadecane		721	2037		–

There are three different types of materials used to construct the porous medium: glass spheres, copper foam, and aluminum foam. The physical properties of the various materials are listed in Table 1.

It is assumed that the suspension is incompressible and the fluid is Newtonian. The unsteady flow and heat transfer behavior of the suspension was taken into account. Moreover, the temperature difference between the foam matrix and the suspension was taken into account using the local thermal non-equilibrium model. The thermal and hydrodynamic behavior of a suspension containing NEPCM particles in a porous media can be represented by the following equations:

$$\frac{\partial u}{\partial x} + \frac{\partial v}{\partial y} = 0 \quad (1)$$

$$\frac{\rho_{nf}}{\varepsilon} \frac{\partial u}{\partial t} + \frac{\rho_{nf}}{\varepsilon^2} \left(u \frac{\partial u}{\partial x} + v \frac{\partial u}{\partial y} \right) = -\frac{\partial p}{\partial x} + \frac{\mu_{nf}}{\varepsilon} \left(\frac{\partial^2 u}{\partial x^2} + \frac{\partial^2 u}{\partial y^2} \right) - \frac{\mu_{nf}}{\kappa} u \quad (2)$$

$$\frac{\rho_{nf}}{\varepsilon} \frac{\partial v}{\partial t} + \frac{\rho_{nf}}{\varepsilon^2} \left(u \frac{\partial v}{\partial x} + v \frac{\partial v}{\partial y} \right) = -\frac{\partial p}{\partial y} + \frac{\mu_{nf}}{\varepsilon} \left(\frac{\partial^2 v}{\partial x^2} + \frac{\partial^2 v}{\partial y^2} \right) + g \rho_{nf} \beta_{nf} (T_{nf} - T_c) - \frac{\mu_{nf}}{\kappa} v \quad (3)$$

$$\varepsilon(\rho C_p)_{nf} \frac{\partial T_{nf}}{\partial t} + (\rho C_p)_{nf} \left(u \frac{\partial T_{nf}}{\partial x} + v \frac{\partial T_{nf}}{\partial y} \right) = \varepsilon k_{nf} \left(\frac{\partial^2 T_{nf}}{\partial x^2} + \frac{\partial^2 T_{nf}}{\partial y^2} \right) + h(T_s - T_{nf}) \quad (4)$$

$$(1 - \varepsilon)(\rho C_p)_s \frac{\partial T_s}{\partial t} = (1 - \varepsilon)k_s \left(\frac{\partial^2 T_s}{\partial x^2} + \frac{\partial^2 T_s}{\partial y^2} \right) - h(T_s - T_{nf}) \quad (5)$$

The employed boundary conditions at the enclosure walls are:

$$\forall x, y, t | x = 0, 0 \leq y \leq L, t > 0 \Rightarrow u = v = 0, T_{nf} = T_s = T_h + a \sin(\omega t) \quad (6a)$$

$$\forall x, y, t | x = L, 0 \leq y \leq L, t > 0 \Rightarrow u = v = 0, T_{nf} = T_s = T_c \quad (6b)$$

$$\forall x, y, t \begin{cases} y = 0, 0 \leq x \leq L, t > 0 \Rightarrow u = v = 0, \frac{\partial T_{nf}}{\partial y} = \frac{\partial T_s}{\partial y} = 0 \\ y = L, 0 \leq x \leq L, t > 0 \Rightarrow u = v = 0, \frac{\partial T_{nf}}{\partial y} = \frac{\partial T_s}{\partial y} = 0 \end{cases} \quad (6c)$$

$$\forall x, y, t | 0 \leq x \leq L, 0 \leq y \leq L, t = 0 \Rightarrow u = u_{st}, v = v_{st}, T_{nf} = T_{nf,st}, T_s = T_{s,st} \quad (6d)$$

where a and ω are the amplitude and wave number for the heated boundary condition. The subscript of st indicates the steady state condition when there is no temperature oscillation, i.e. $a = 0$.

2.1. Suspension bulk properties

The density of suspension is computed following the mass conservation law as [40,41]:

$$\rho_{nf} = (1 - \phi)\rho_{bf} + \phi\rho_p \quad (7)$$

where ϕ is the concentration of nanoparticles, and ρ is the density. The subscripts *nf*, *bf*, and *p* indicate the NEPCM suspension, host fluid, and nanoparticles, respectively.

NEPCM particles density reads [40,41]:

$$\rho_p = \frac{(1 + \iota)\rho_{co}\rho_{sh}}{\rho_{sh} + \iota\rho_{co}} \quad (8)$$

The specific heat capacity of the suspension can be calculated as [42,43]:

$$C_{p,nf} = \frac{(1 - \phi)(\rho C_p)_{bf} + \phi(\rho C_p)_{p,eff}}{\rho_{nf}} \quad (9)$$

where the effective specific heat, i.e. $C_{p,p,eff}$ of the nano-encapsulated particles with no phase change is equal to the sensible heat capacity, i.e. $C_{p,p}$ [40,41]:

$$(\rho C_p)_p = \frac{(C_{p,co} + \iota C_{p,sh})\rho_{co}\rho_{sh}}{(\rho_{sh} + \iota\rho_{co})} \quad (10)$$

When the core of the nanoparticles experiences a phase transition, the latent heat of change phase is absorbed by the specific heat capacity of the nanoparticles, resulting in an increase in specific heat capacity.

$$C_{p,p,eff} = C_{p,p} + \left\{ \frac{\pi}{2} \cdot \left(\frac{h_{sf}}{T_{Mr}} - C_{p,p} \right) \cdot \sin \left(\pi \frac{T_{nf} - T_0}{T_{Mr}} \right) \right\} \begin{cases} 0 & T_{nf} < T_0 \\ 1 & T_0 < T_{nf} < T_1 \\ 0 & T_{nf} > T_1 \end{cases} \quad (11)$$

T_0 and T_1 are respectively the down and top margins of the melting bond T_{Mr} :

$$\begin{cases} T_0 = T_{fu} - T_{Mr}/2 \\ T_1 = T_{fu} + T_{Mr}/2 \end{cases} \quad (12)$$

For the mixture, the thermal volume expansion coefficient is expressed as [33,40]:

$$\beta_{nf} = (1 - \phi)\beta_{bf} + \phi\beta_p \quad (13)$$

The linear relationships are adopted to calculate the thermal conductivity and dynamic viscosity of the NEPCM mixture [40,44]:

$$\frac{k_{nf}}{k_{bf}} = 1 + N_c\phi \quad (14a)$$

$$\frac{\mu_{nf}}{\mu_{bf}} = 1 + N_v\phi \quad (14b)$$

N_c and N_v are the numbers of thermal conductivity and dynamic viscosity. The relations of Equation (14) could be valid for diluted nanofluids, i.e. $\phi \leq 0.5\%$.

2.2. Non-dimensional form of governing equations

The following parameters are invoked to dimensionalize Equations (1)–(5) and the corresponding boundary conditions Equation (6):

$$\begin{aligned} X = \frac{x}{L}, Y = \frac{y}{L}, U = \frac{uL}{\alpha_{bf}}, V = \frac{vL}{\alpha_{bf}}, P = \frac{pL^2}{\rho_{bf}\alpha_{bf}^2}, \\ \theta_{nf} = \frac{T_{nf} - T_c}{T_h - T_c}, \theta_s = \frac{T_s - T_c}{T_h - T_c}, \tau = \frac{\alpha_f t}{L^2}, A = \frac{a}{T_h - T_c} \end{aligned} \quad (15)$$

Hence, we then have:

$$\frac{\partial U}{\partial X} + \frac{\partial V}{\partial Y} = 0 \quad (16)$$

$$\varepsilon^{-2} \rho_r \left(\varepsilon \frac{\partial U}{\partial \tau} + U \frac{\partial U}{\partial X} + V \frac{\partial U}{\partial Y} \right) = - \frac{\partial P}{\partial X} + Pr \varepsilon^{-1} \mu_r \left(\frac{\partial^2 U}{\partial X^2} + \frac{\partial^2 U}{\partial Y^2} \right) - \frac{Pr}{Da} \mu_r U \quad (17)$$

$$\begin{aligned} \varepsilon^{-2} \rho_r \left(\varepsilon \frac{\partial V}{\partial \tau} + U \frac{\partial V}{\partial X} + V \frac{\partial V}{\partial Y} \right) = - \frac{\partial P}{\partial Y} + Pr \varepsilon^{-1} \mu_r \left(\frac{\partial^2 V}{\partial X^2} + \frac{\partial^2 V}{\partial Y^2} \right) \\ + Ra \cdot Pr \beta_r \rho_r \theta - \frac{Pr}{Da} \mu_r V \end{aligned} \quad (18)$$

The dimensionless numbers in Equations (17) and (18) denote the Rayleigh number (Ra), the Prandtl number (Pr), and the Darcy number (Da), respectively, which are introduced as:

$$Ra = \frac{g \rho_{bf} \beta_{bf} \Delta T L^3}{\alpha_{bf} \mu_{bf}}, Pr = \frac{\mu_{bf}}{\rho_{bf} \alpha_{bf}}, Da = \frac{K}{L^2} \quad (19)$$

Also,

$$\mu_r = 1 + Nv\phi, \rho_r = \left(\frac{\rho_b}{\rho_f} \right) = (1 - \phi) + \phi \left(\frac{\rho_{nf}}{\rho_{bf}} \right), \beta_r = \left(\frac{\beta_{nf}}{\beta_{bf}} \right) = (1 - \phi) + \phi \left(\frac{\beta_{nf}}{\beta_{bf}} \right) \quad (20)$$

By assuming equivalent thermal expansion behavior for both of particles and the base fluid, the expansion ratio could be adopted as $\beta_r = 1$.

$$Cr \left(\varepsilon \frac{\partial \theta_{nf}}{\partial \tau} + U \frac{\partial \theta_{nf}}{\partial X} + V \frac{\partial \theta_{nf}}{\partial Y} \right) = \varepsilon k_{r,nf} \left(\frac{\partial^2 \theta_{nf}}{\partial X^2} + \frac{\partial^2 \theta_{nf}}{\partial Y^2} \right) + H(\theta_s - \theta_{nf}) \quad (21)$$

where

$$k_{r,nf} = \left(\frac{k_{nf}}{k_{bf}} \right), Cr = \frac{(\rho C_p)_{nf}}{(\rho C_p)_{bf}} = (1 - \phi) + \phi \lambda + \frac{\phi}{\delta Ste} f \quad (22)$$

Here, Cr is the ratio of the suspension heat capacity to the sensible heat capacity of the base fluid. The Stefan number (Ste), the non-dimensional melting interval (δ), and the sensible

heat capacity ratio (λ) read:

$$\lambda = \frac{(C_{p,c} + \iota C_{p,sh})\rho_c \rho_{sh}}{(\rho C_p)_{bf}(\rho_{sh} + \iota \rho_c)}, \quad \delta = \frac{T_{Mr}}{\Delta T}, \quad Ste = \frac{(\rho C_p)_{bf} \Delta T (\rho_{sh} + \iota \rho_c)}{(h_{sf} \rho_c \rho_{sh})} \quad (23)$$

Furthermore, the non-dimensional fusion function (f) is represented as a function of non-dimensional temperature, as follows:

$$f = \frac{\pi}{2} \sin \left(\frac{\pi}{\delta} (\theta - \theta_f + \delta/2) \right) \times \begin{cases} 0 & \theta < \theta_f - \delta/2 \\ 1 & \theta_f - \delta/2 < \theta < \theta_f + \delta/2 \\ 0 & \theta > \theta_f + \delta/2 \end{cases} \quad (24)$$

Where, θ_f , denotes the dimensionless fusion temperature, which reads:

$$\theta_f = \frac{T_{fu} - T_c}{T_h - T_c} \quad (25)$$

The conservation of energy in the solid porous matrix is achieved in the following non-dimensional form:

$$(1 - \varepsilon) \frac{(\rho C_p)_s}{(\rho C_p)_{bf}} \frac{\partial \theta_s}{\partial \tau} = (1 - \varepsilon) K_{r,s} \left(\frac{\partial^2 \theta_s}{\partial X^2} + \frac{\partial^2 \theta_s}{\partial Y^2} \right) - H(\theta_s - \theta_{nf}) \quad (26)$$

where

$$K_{r,s} = \frac{k_s}{k_{bf}}, H = \frac{hL^2}{k_{bf}} \quad (27)$$

Ultimately, the corresponding dimensionless forms of the boundary conditions is reached as:

$$\text{At the left wall : } U = V = 0, \theta_{nf} = \theta_s = 1 + A \sin(\Omega \tau) \quad (28a)$$

$$\text{At the right wall : } U = V = 0, \theta_{nf} = \theta_s = 0 \quad (28b)$$

$$\text{At top and bottom walls : } \frac{\partial \theta_{nf}}{\partial Y} = \frac{\partial \theta_s}{\partial Y} = 0 \quad (28c)$$

$$\text{Initial conditions } U = U_{st}, V = V_{st}, \theta_{nf} = \theta_{nf,st}, \theta_s = \theta_{s,st} \quad (28d)$$

where subscript st shows the steady state solution when $A = 0$, and Ω denotes the non-dimensionalized frequency, $\Omega = \omega L^2 / \alpha_f$.

2.3. Rated of heat transfer

The average Nusselt numbers for the liquid and porous matrix are introduced for the hot wall as:

$$Nu_{nf,\tau} = k_{r,nf} \int_0^1 \left(\frac{\partial \theta_{nf}}{\partial X} \right) dY \quad (29a)$$

$$Nu_{s,\tau} = K_{r,s} \int_0^1 \left(\frac{\partial \theta_s}{\partial X} \right) dY \quad (29b)$$

The time-averaged Nusselt numbers are identified over a period of wall temperature oscillation τ_p ($\tau_p = 2\pi/\Omega$) as:

$$Nu_{nf,a} = \frac{1}{\tau_p} \int_{n\tau_p}^{(n+1)\tau_p} \int_0^1 Nu_{nf,\tau} dY d\tau \quad (30a)$$

$$Nu_{s,a} = \frac{1}{\tau_p} \int_{n\tau_p}^{(n+1)\tau_p} \int_0^1 Nu_{s,\tau} dY d\tau \quad (30b)$$

Finally, the streamlines, which may be used to depict the suspension flow, are calculated by solving the following Poisson equation:

$$\frac{\partial^2 \Psi}{\partial X^2} + \frac{\partial^2 \Psi}{\partial Y^2} = - \left(\frac{\partial V}{\partial X} - \frac{\partial U}{\partial Y} \right) \quad (31)$$

where the Dirichlet boundary condition with zero value was considered as the boundary conditions.

3. Numerical analysis and grid evaluation

3.1. Numerical method

The governing equations in the previous section are non-linear, and they were modified to a weaker form to be solved. Galerkin finite element method (FEM) was utilized to integrate weaker form equations within the domain study. This method is detailed and explained in Ref. [45].

3.2. Grid study and independency

Achieving accurate and correct answers in each numerical study mainly depend on the quality provided grid within the domain study. So, six different grid sizes were provided inside the cavity as listed in Table 2. The average Nusselt number of the suspension and glass balls was examined for all grids when $Ste = 0.5$, $\theta_f = 0.5$, $Ra = 10^7$, $Nc = 23.8$, $\lambda = 0.32$, $H = 10$, $\phi = 0.03$, $\Omega = \pi/6$, $A = 0.5$, $Da = 10^{-4}$, $\epsilon = 0.8$, $Nv = 12.5$, and $Pr = 6.2$. It was noticed that the average Nusselt number values are equal for fifth (250×250) and sixth (300×300) grid sizes. So, the fifth one was chosen for the whole numerical simulations in order to decrease the cost and duration of simulations.

Moreover, it should be noted that the average Nusselt number for the solid phase ($Nu_{s,a}$) is not much sensitive to the mesh size but the average Nusselt number for the NEPCM suspension ($Nu_{nf,a}$) is slightly changed by the change of mesh size. The partial differential equation for solid phase is generally governed by the conduction heat transfer without ant advection term. It is only linked to the NEPCM suspensions through source terms. Hence, it is easy to solve and converge. However, the heat transfer equation for the suspension contains advective terms directly connected to the NEPCM suspension and the phase change of nanoparticles. Thus, the change of grid size influences the heat transfer in the suspension phase ($Nu_{nf,a}$) more than that of the solid phase ($Nu_{s,a}$) (Table 2) .

Table 2. Grid size influence on the average Nusselt number of the suspension and glass balls when $Ste = 0.5$, $\theta_f = 0.5$, $Ra = 10^7$, $Nc = 23.8$, $\lambda = 0.32$, $H = 10$, $\phi = 0.03$, $\Omega = \pi/6$, $A = 0.5$, $Da = 10^{-4}$, $\epsilon = 0.8$, $Nv = 12.5$, and $Pr = 6.2$.

Nusselt number	Grid size					
	50×50	100×100	150×150	200×200	250×250	300×300
$Nu_{s,a}$	0.677	0.676	0.676	0.676	0.676	0.676
$Nu_{nf,a}$	10.461	10.432	10.428	10.425	10.424	10.424

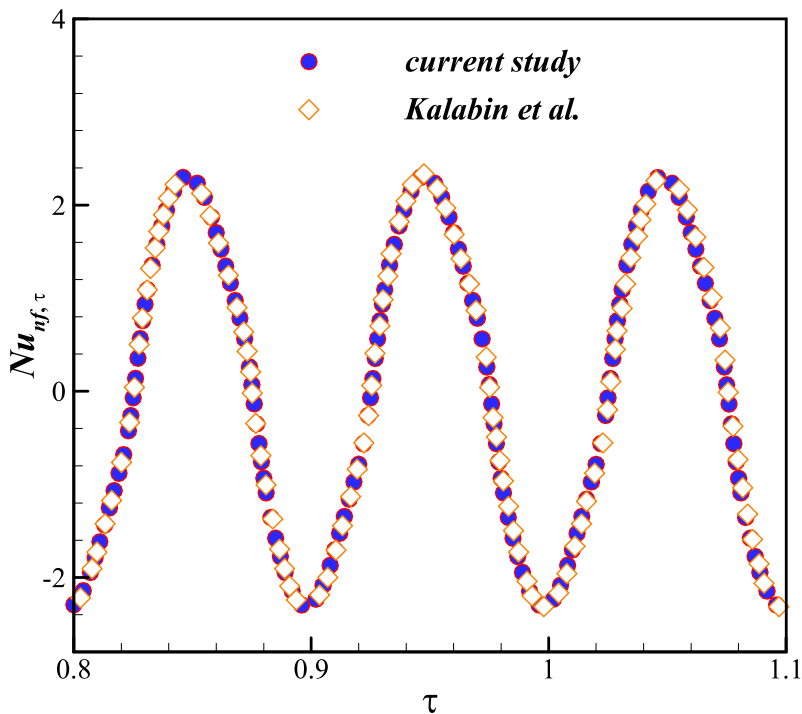


Figure 2. The average Nusselt number over time resulted from the study done by Kalabin et al. [46] and that of our study for $Ra = 2 \times 10^5$, $Pr = 1$, $\phi = 0.0$, $\epsilon = 1$.

3.3. Validation

The results of the current investigation were compared with other similar works to validate the method used. In the first case, the correctness of this study was examined by being compared to the research of Kalabin et al. [46]. They numerically studied the free convection inside an air-filled cavity. The cavity horizontal walls were insulated, and one of the vertical walls had a constant temperature while the other wall had various temperatures. Figure 2 depicts the average Nusselt number of two studies at various time-steps when $Ra = 2 \times 10^5$, $Pr = 1$, $\phi = 0.0$, $\epsilon = 1$.

An agreement is seen between the outcomes of the two studies. As the second step, a comparison was performed between this study and the research of Calcagni et al. [47]. They did a numerical and experimental investigation on natural convection within a square

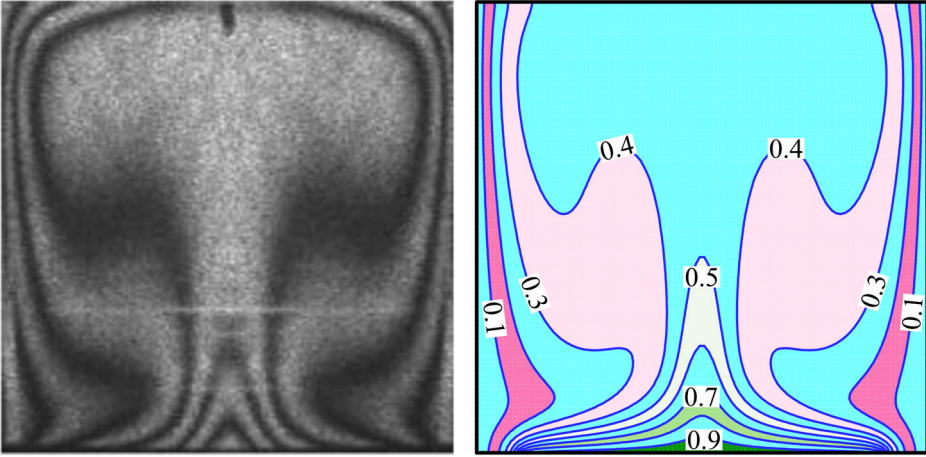


Figure 3. comparison between the temperature contour of the experimental work of (a) Calcagni et al. [47] and (b) the current numerical study at $Pr = 0.71$, $\phi = 0.0$, $\epsilon = 1$ and $Ra = 1.425 \times 10^5$.

enclosure in which the bottom wall was exposed to an outside heater. The walls of the cavity acted as cooling parts and the top wall was insulated.

Figure 3 demonstrates the temperature contours in the enclosure of the current study and experimental results of Ref. [47] when $Pr = 0.71$, $\phi = 0.0$, $\epsilon = 1$ and $Ra = 1.425 \times 10^5$. As seen, results of two studies indicates desirable agreement. Finally, the outcomes of this research were compared to the results of the work of Baytas and Pop [48]. They examined the natural convection in a porous square cavity where the non-equilibrium model of thermal energy transport was assumed. Two vertical walls of their research were isotherms (T_h and T_c), and horizontal walls were considered adiabatic. A fine agreement is observed between the results of two studies according to Figure 4, which illustrates the average Nusselt number of solid and fluid phases versus non-dimensional interface heat transfer coefficient.

4. Outcomes and discussions

The numerical results of the modeled problem are represented in this portion. Indeed, the effects of the alterable factors on flow and temperature fields, the heat capacity ratio contours, and the heat transfer characteristics of the suspension and the solid matrix are studied. The ranges of the alterable parameters are: Stefan number $0.2 \leq Ste \leq \infty$, the dimensionless fusion temperature $0.05 \leq \theta_f \leq 1$, the interface heat transfer coefficient $1 \leq H \leq 1000$, the non-dimensional frequency of the temperature profile $0.01\pi \leq \Omega \leq \pi$, the non-dimensional amplitude of the temperature profile $0.0 \leq A \leq 1$, and the NEPCM volumetric fraction $0.0 \leq \phi \leq 5\%$. It's important to note that the other non-dimensional parameters are fixed so that $Ra = 10^7$, $Da = 10^{-4}$, $\epsilon = 0.8$, $Nc = 23.8$, $Nv = 12.5$, $\lambda = 0.32$, and $Pr = 6.2$. Default Case for the aluminum and copper foams as well as the glass balls is $Ste = 0.5$, $\theta_f = 0.5$, $Ra = 10^7$, $H = 10$, $\phi = 0.03$, $\Omega = \pi/6$, $A = 0.5$.

Results in terms of contours of streamlines, isotherms, and the heat capacity ratio for several snapshots during an oscillation period are illustrated in Figure 5 that correspond to the

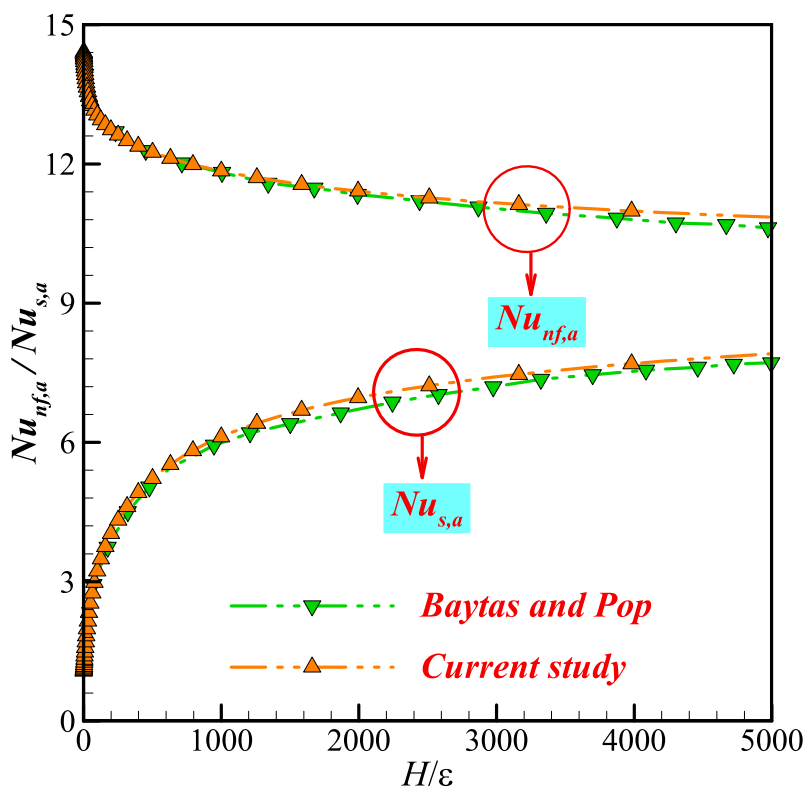


Figure 4. The average Nusselt numbers of the two phases as obtained by Baytas and Pop [48] and in our study.

aluminum foam in the default case. Notice that in all of the time instants, a clockwise vortex is formed inside the cavity having an ascending flow near the hot (left) wall and a descending flow near the cold (right) wall. This vortex is responsible for the advection of heat and the circulation of the NEPCM particles along with the host fluid inside the cavity. Inspection of the temperature contours indicates a high degree of LTNE between the NEPCM suspension and the solid matrix since the patterns of the contour lines of the components are completely different at the all-time instants. Notice that, in spite of the vortex formed in the NEPCM suspension, the isotherms of the solid matrix are almost vertical. It is evident that the highest values of the flow strength and the temperatures belong to $\tau = T/4$ while the lowest values appear at $\tau = 3T/4$. This is not surprising since the hot wall attains its maximum temperature at $\tau = T/4$ while its minimum temperature is reached at $\tau = 3T/4$.

The NEPCM particles experience hot and cold regions during their circulation inside the cavity. When a NEPCM particle enters a region having a temperature greater than its fusion temperature, it melts. The molten particle, however, undergoes a phase change to a solid state after entering a region colder than its fusion temperature. For the current case with $\phi = 0.03$, the heat capacity ratio takes the value of 0.98 in the regions where the NEPCM suspension acquires a temperature higher or lower than the melting point of the NEPCM particles. Hence, the deviation of Cr from 0.98 reflects the phase change of the NEPCM particles. Thereby, each red ribbon in Figure 5 shows the phase change zone at a snapshot

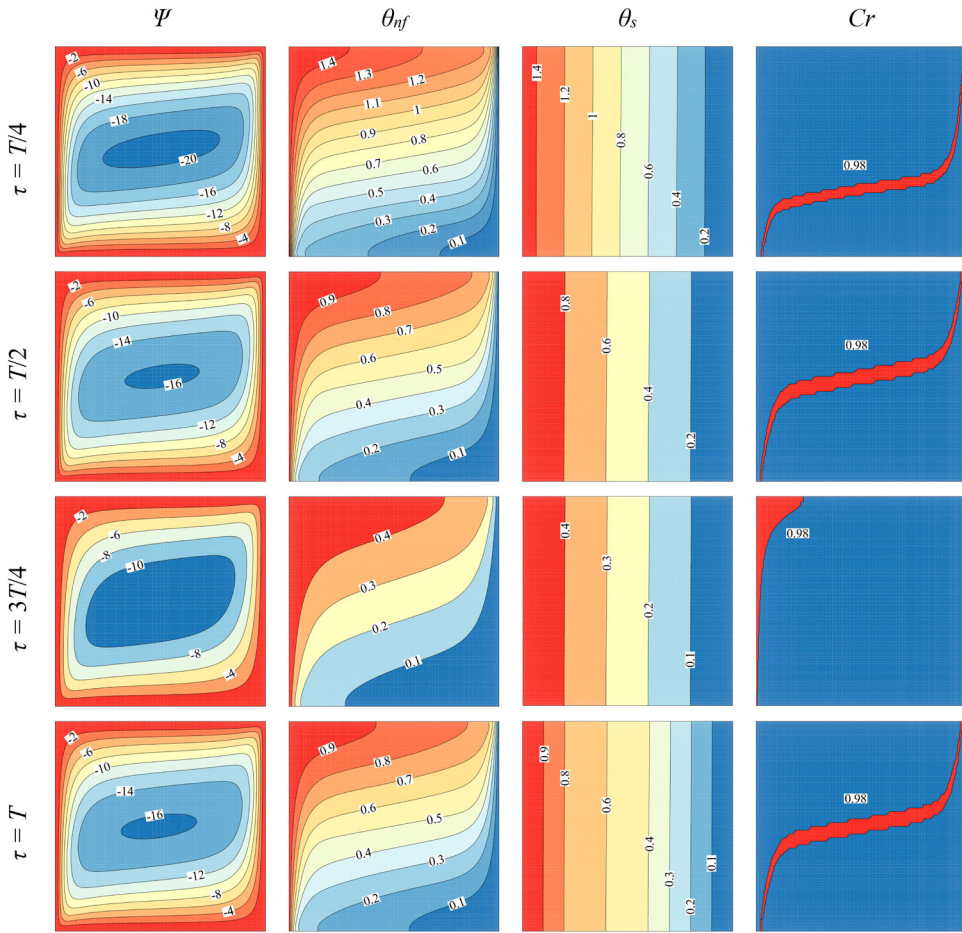


Figure 5. Streamlines and isothermal contours of the fluid and solid phases of the porous media and heat capacity ratio at four snapshots during an oscillation period for the aluminum foam.

during an oscillation period, separating the molten NEPCM particles from the solidified ones. Scrutiny of the figure shows that at $\tau = 3 T/4$, which corresponds to the hot wall lowest temperature, the phase change ribbon is pushed towards the hot (left) wall, and most of the cavity is occupied by the NEPCM particles in the solid phase.

Figure 6 depicts the instantaneous Nusselt number variations for the NEPCM particles and the solid matrix for the matrix being made up of aluminum foam, copper foam, or glass balls. The figure demonstrates that for the metallic foams, the heat transfer of the medium is substantially higher than the NEPCM particles. However, the opposite trend is observed for the glass balls, which is expected. It is also shown that the Nusselt number of copper foam is about two times higher than the aluminum foam. Notice that change of the solid matrix material may not change the Nusselt number of the NEPCM suspension substantially.

The dependency of the average Nusselt number of the components to the non-dimensional fusion temperature and the non-dimensional amplitude of the temperature profile is portrayed in Figures 7–9, which correspond to the aluminum foam, the copper

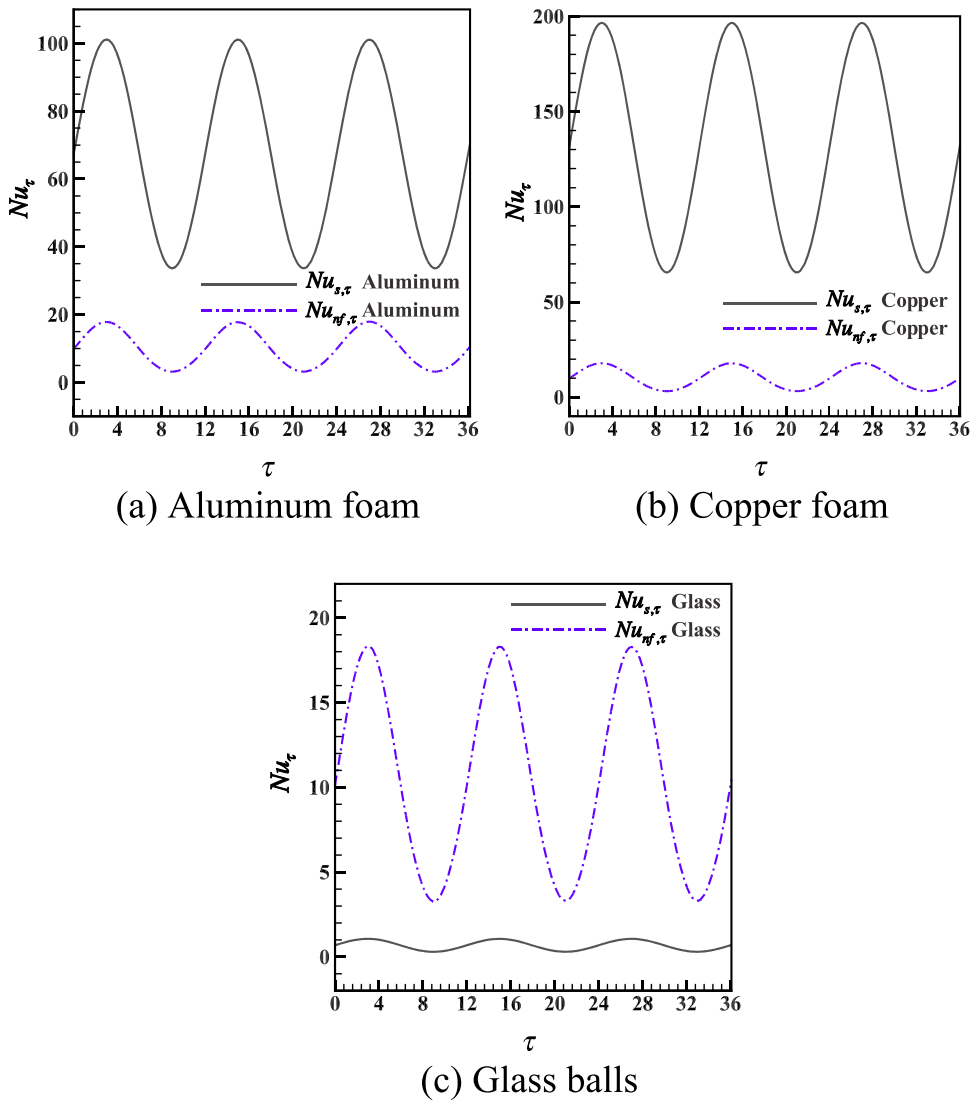
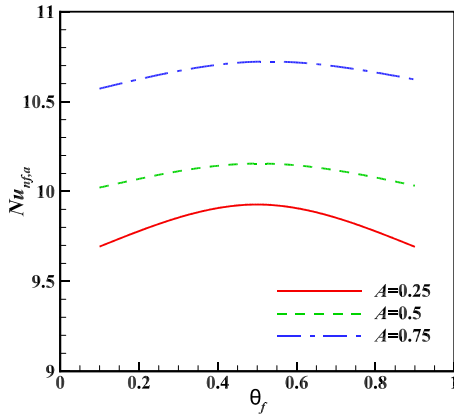
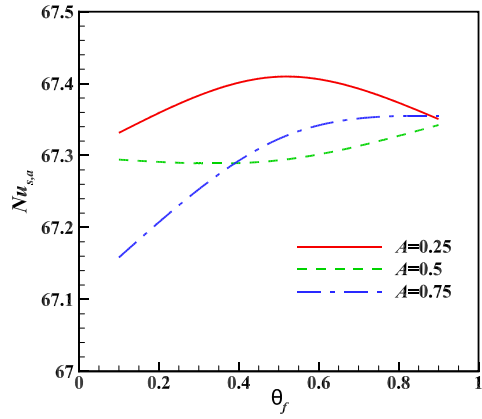


Figure 6. Instantaneous Nusselt number variations for the NEPCM suspension and the solid matrix for different porous matrix materials.

foam, and the glass balls, respectively. The figures show that for all of the current solid matrices, the Nusselt number of the NEPCM suspension achieves its maximum value at $\theta_f = 0.5$. However, notice that no general conclusion can be drawn about the effect of the fusion temperature on the Nusselt number of the solid matrix. It is evident that a rise in the dimensionless amplitude of the temperature profile elevates the Nusselt number of the NEPCM suspension. Regarding the Nusselt number of the solid matrix, the trend is more complex. For most of the cases using the metallic foams, it can be noticed that the Nusselt number of the solid matrix is a decreasing function of the non-dimensional amplitude of the temperature profile; however, a nearly direct relation exists between them, for the glass balls. Figure 7 shows an increasing trend of $Nu_{s,a}$ by an increase of fusion temperature when

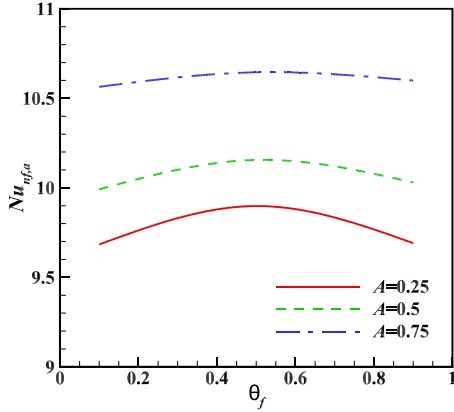


(a) NEPCM suspension

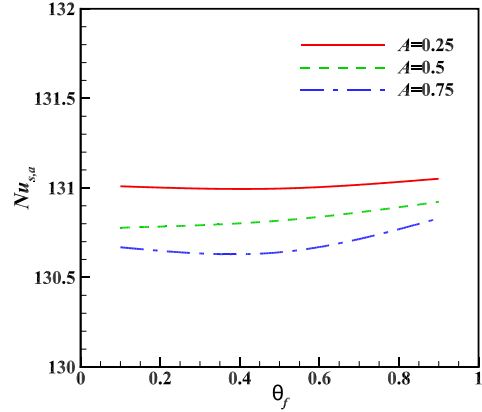


(b) Solid matrix

Figure 7. Relationship of the average Nusselt number of the components with the dimensionless fusion temperature and the dimensionless amplitude of the temperature profile for the aluminum foam.



(a) NEPCM suspension



(b) Solid matrix

Figure 8. Relationship of the average Nusselt number of the components with the dimensionless fusion temperature and the dimensionless amplitude of the temperature profile for the copper foam.

$A = 0.75$. However, for the other two cases, no monotonic trend could be found. Indeed, an increase in temperature amplitude elevates the local temperature next to the wall and shifts the location of phase change toward the heated wall. Thus, as seen, the heat transfer improves. However, for small temperature amplitudes, the phase change occurs in the central area of the enclosure, and depending on its distance to the heated or cold wall, the Nusselt number could be changed.

Figures 10–12 indicate the dependency of the heat transfer of the components to the dimensionless fusion temperature and the non-dimensional frequency of the temperature profile for the aluminum foam, the copper foam, and the glass balls, respectively. Again, notice that the Nusselt number of the NEPCM suspension achieves its maximum value at $\theta_f = 0.5$. However, the trend of the Nusselt number is more complex for the solid matrices.

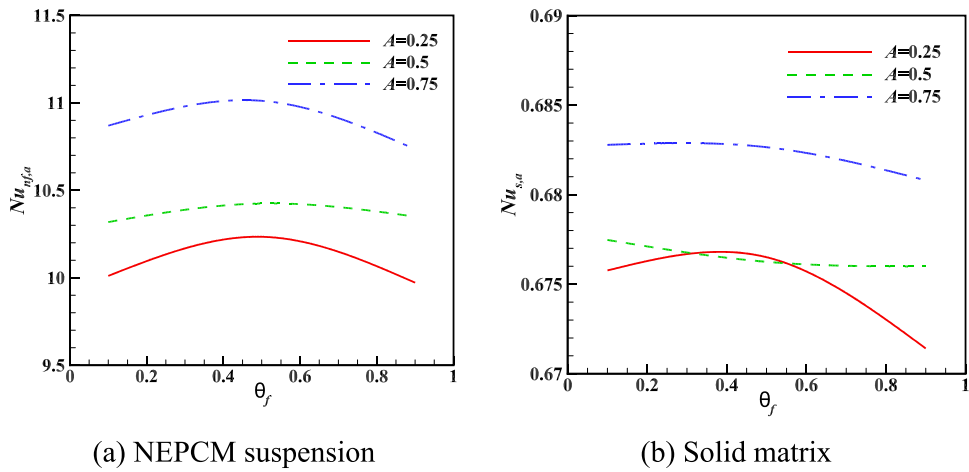


Figure 9. Relationship of the time-averaged Nusselt number of the components to the non-dimensional fusion temperature and the non-dimensional amplitude of the temperature profile for the glass balls.

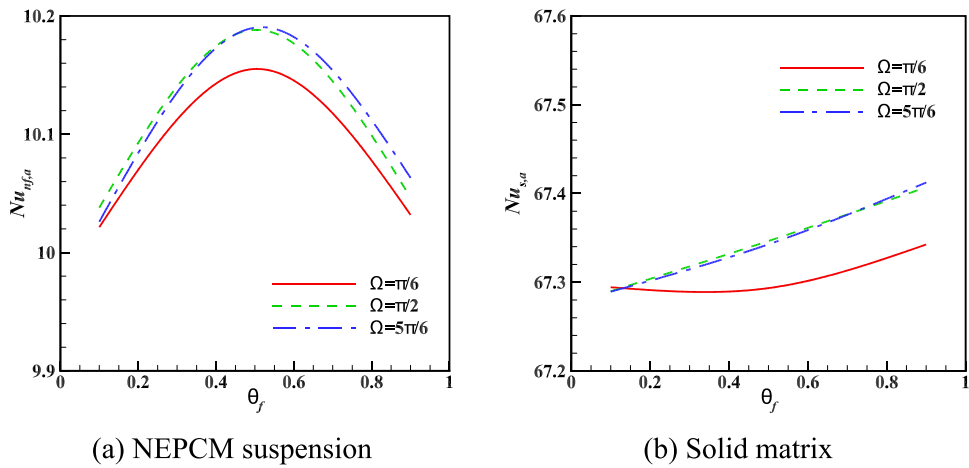


Figure 10. Average Nusselt number variations for the components as a function of the fusion temperature for different frequencies of the temperature profile for the aluminum foam.

A comparison of these figures with Figures 7–9 shows that the amplitude of the temperature profile is more influential on the heat transfer performance than its frequency. Notice that an increment in the dimensionless frequency of the temperature profile improves the Nusselt number of the NEPCM suspension. However, this effect is negligible when copper foam is used. However, notice that no general conclusion can be drawn about the impact of the dimensionless frequency of the temperature profile on the Nusselt number of the solid matrix.

Finally, a parameterized analysis is carried out to investigate the effects of various non-dimensional factors on the time-averaged Nusselt number of the components. Results for the aluminum foam, the copper foam, and the glass balls are outlined in Tables 3–5,

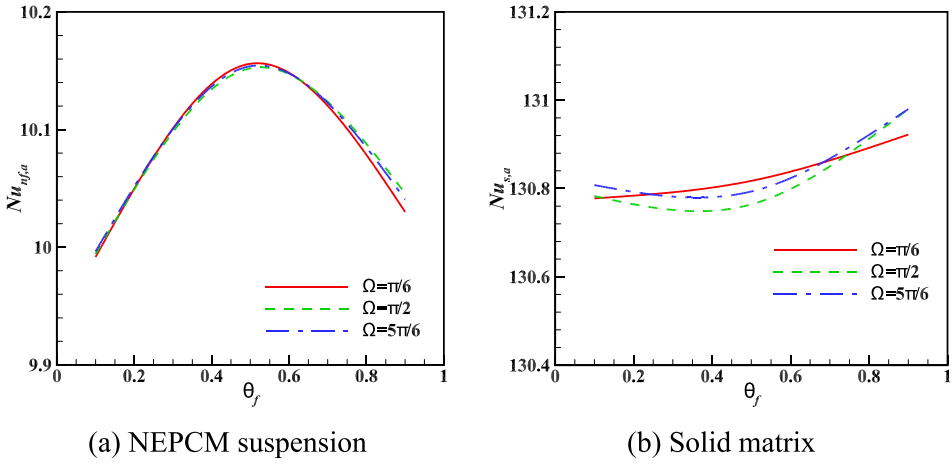


Figure 11. Dependency of the average Nusselt number of the components on the non-dimensional fusion temperature and the non-dimensional frequency of the temperature profile for the copper foam.

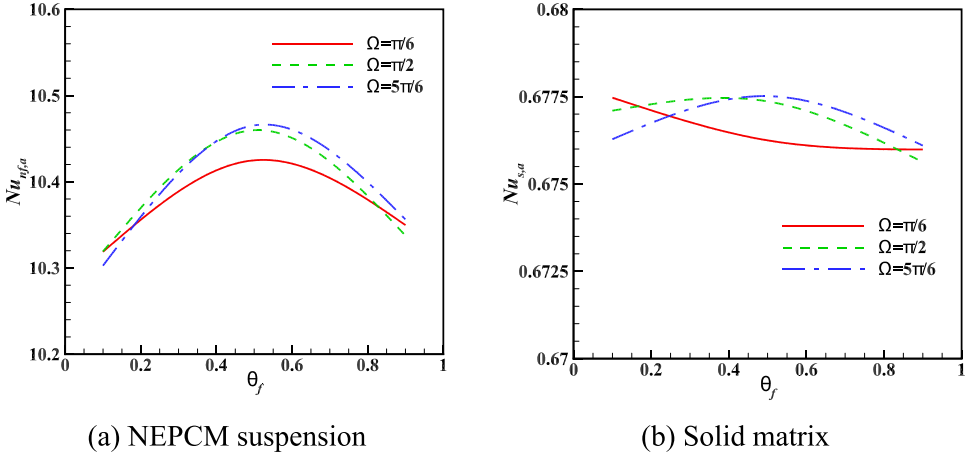


Figure 12. Dependency of the time-averaged Nusselt number of the components to the dimensionless fusion temperature and the dimensionless frequency of the temperature profile for the glass balls.

respectively. It is evident that adding 3% of the NEPCM particles to the host fluid, the Nusselt number of the fluid reduces by about 4% in the aluminum foam while elevating by about 17% and 36% in the copper foam and the glass balls, respectively. However, this particle addition may not bring more than 1% variations in the Nusselt number of the metallic foams; but it is accompanied by 8% reduction in the Nusselt number of the glass balls.

Inspection of the results shows that raising the Stefan number from 0.5 to 5×10^5 and elevating the dimensionless fusion temperature from 0.5 to 0.9 decrease the Nusselt number of the NEPCM particles by about 3% and 1%, respectively. However, their effects on the Nusselt number of the solid matrices may not exceed 0.1%. It is found that an increment of the non-dimensional interface heat transfer coefficient from 10 to 1000 is accompanied by a diminishment of the Nusselt number of the NEPCM particles and elevation of heat transfer

Table 3. Effects of different factors on the time-averaged Nusselt number for the aluminum foam.

Case	Ste	θ_f	H	ϕ	Ω	A	$Nu_{nf,a}$	$Nu_{s,a}$
0	0.5	0.5	10	0.00	$\pi/6$	0.5	8.650	67.360
1	0.5	0.5	10	0.03	$\pi/6$	0.5	10.155	67.293
2	5×10^5	0.5	10	0.03	$\pi/6$	0.5	9.836	67.333
3	0.5	0.9	10	0.03	$\pi/6$	0.5	10.032	67.342
4	0.5	0.5	1000	0.03	$\pi/6$	0.5	2.861	76.100
5	0.5	0.5	10	0.05	$\pi/6$	0.5	10.638	67.208
6	0.5	0.5	10	0.03	$2\pi/3$	0.5	10.158	67.283
7	0.5	0.5	10	0.03	$\pi/6$	1.0	11.506	67.129

Table 4. Effects of different factors on the time-averaged Nusselt number for the copper foam.

Case	Ste	θ_f	H	ϕ	Ω	A	$Nu_{nf,a}$	$Nu_{s,a}$
0	0.5	0.5	10	0.00	$\pi/6$	0.5	8.652	130.883
1	0.5	0.5	10	0.03	$\pi/6$	0.5	10.156	130.817
2	5×10^5	0.5	10	0.03	$\pi/6$	0.5	9.834	130.914
3	0.5	0.9	10	0.03	$\pi/6$	0.5	10.030	130.922
4	0.5	0.5	1000	0.03	$\pi/6$	0.5	25.72	138.958
5	0.5	0.5	10	0.05	$\pi/6$	0.5	10.630	130.649
6	0.5	0.5	10	0.03	$2\pi/3$	0.5	10.156	130.806
7	0.5	0.5	10	0.03	$\pi/6$	1.0	11.506	130.507

Table 5. Effects of different factors on the time-averaged Nusselt number for the glass balls.

Case	Ste	θ_f	H	ϕ	Ω	A	$Nu_{nf,a}$	$Nu_{s,a}$
0	0.5	0.5	10	0.00	$\pi/6$	0.5	8.934	0.738
1	0.5	0.5	10	0.03	$\pi/6$	0.5	10.425	0.676
2	5×10^5	0.5	10	0.03	$\pi/6$	0.5	10.088	0.671
3	0.5	0.9	10	0.03	$\pi/6$	0.5	10.350	0.676
4	0.5	0.5	1000	0.03	$\pi/6$	0.5	9.705	2.078
5	0.5	0.5	10	0.05	$\pi/6$	0.5	10.887	0.642
6	0.5	0.5	10	0.03	$2\pi/3$	0.5	10.435	0.677
7	0.5	0.5	10	0.03	$\pi/6$	1.0	11.775	0.692

in the solid matrices. The percentages of the diminishments are 72%, 75%, 7%, and the percentages of the elevations are 13%, 6%, 207% for the solid matrix made up of the aluminum foam, the copper foam, and the glass balls, respectively.

Scrutiny of the results demonstrates that with a rise in NEPCM volumetric fraction from 3% to 5%, the Nusselt number of the suspension boosts by about 4%. For the metallic foams, however, this effect is not influential on the heat transfer in the solid matrix; but it elevates the Nusselt number of the glass balls by about 5%. Among the current alterable parameters, the lowest contribution belongs to the non-dimensional frequency of the temperature profile, which may not change the results by more than 0.2%. It is evident that duplicating the amplitude of the temperature profile boosts the Nusselt number of the NEPCM particles by about 13%. For the metallic foams, this may not change the heat transfer of the solid matrix by more than 0.3%. However, it elevates the Nusselt number of glass balls by about 2%.

5. Conclusion

Unsteady free convection of a NEPCM-water suspension in a square porous cavity was simulated and discussed in this study. In order to do this, a two-temperature LTNE model was used, with the temperature differential between the NEPCM particles and the solid matrix taken into account. The non-dimensional governing differential equations were solved through the finite element method. Computations were undertaken for aluminum foam, copper foam, and glass balls as the solid matrix, and the corresponding results were compared under different conditions. The key findings of this investigation are summarized below:

- (1) When the hot wall temperature reaches its minimum value during an oscillation period, most of the cavity is occupied by the NEPCM particles in the solid phase.
- (2) For the metallic foams, the Nusselt number of the solid matrix is substantially higher than the NEPCM particles.
- (3) The heat transfer of the glass balls is much lower than the NEPCM particles.
- (4) The Nusselt number of copper foam is about two times higher than the aluminum foam.
- (5) Although no general conclusion can be drawn for the effect of the fusion temperature on the solid matrix Nusselt number, the heat transfer rate of the NEPCM suspension achieves its maximum value at $\theta_f = 0.5$.
- (6) A rise in the frequency or amplitude of the temperature profile elevates the Nusselt number of the NEPCM suspension.
- (7) For the metallic foams, the Nusselt number of the solid matrix is a decreasing function of the non-dimensional amplitude of the temperature profile. However, a direct relation exists between them for the glass balls.
- (8) Among the current alterable parameters such as the Stefan number, fusion temperature, interfacial heat transfer coefficient, NEPCM volumetric fraction, solid matrix type, and frequency and magnitude of the temperature profile, only the non-dimensional interfacial heat transfer coefficient and the amplitude of the temperature profile make significant contributions to the temperature profile.

The current research focused on the heat transfer aspect of NEPCM suspensions by considering the thermal interaction between the porous medium and the suspension. However, NEPCM suspensions in porous media could be utilized for thermal energy storage as well. Therefore, investigating these suspensions' thermal energy storage behavior could be the subject of future studies.

Authors statement

M. Ghalambaz: Conceptualization, Methodology, Writing – Review & Editing, Investigation, Validation. **S. A. M. Mehryan:** Methodology, Writing – Original draft preparation, Supervision, Writing – Review & Editing. **M. Vaezi:** Conceptualization, Methodology, Writing – Review & Editing, Investigation, Validation. **I. Zahmatkesh:** Methodology, Writing – Original draft preparation, Writing – Review & Editing. **A. Hajjar:** Methodology, Writing – Original draft preparation, Writing – Review & Editing, Investigation. **O. Younis:**

Methodology, Writing – Original draft preparation, Writing – Review & Editing. **M. Ghalambaz:** Methodology, Writing – Original draft preparation, Writing – Review & Editing, Supervision.

Disclosure statement

No potential conflict of interest was reported by the author(s).

References

- [1] Gharbi S, Harmand S, Jabrallah SB. Experimental comparison between different configurations of PCM based heat sinks for cooling electronic components. *Appl Therm Eng.* [2015](#);87:454–462.
- [2] Evola G, Marletta L, Sicurella F. A methodology for investigating the effectiveness of PCM wallboards for summer thermal comfort in buildings. *Build Environ.* [2013](#);59:517–527.
- [3] Moreno P, Solé C, Castell A, et al. The use of phase change materials in domestic heat pump and air-conditioning systems for short term storage: a review. *Renewable Sustainable Energy Rev.* [2014](#);39:1–13.
- [4] Lin Y, Jia Y, Alva G, et al. Review on thermal conductivity enhancement, thermal properties and applications of phase change materials in thermal energy storage. *Renewable Sustainable Energy Rev.* [2018](#);82:2730–2742.
- [5] Sheikholeslami M, Mahian O. Enhancement of PCM solidification using inorganic nanoparticles and an external magnetic field with application in energy storage systems. *J Clean Prod.* [2019](#);215:963–977.
- [6] Su W, Darkwa J, Kokogiannakis G. Review of solid–liquid phase change materials and their encapsulation technologies. *Renewable Sustainable Energy Rev.* [2015](#);48:373–391.
- [7] Mohebbi R, Delouei AA, Jamali A, et al. Pore-scale simulation of non-newtonian power-law fluid flow and forced convection in partially porous media: thermal lattice Boltzmann method. *Physica A.* [2019](#);525:642–656.
- [8] Ismael MA, Ghalib HS. Double diffusive natural convection in a partially layered cavity with inner solid conductive body. *Sci Iran.* [2018](#);25:2643–2659.
- [9] Miroshnichenko IV, Sheremet MA, Oztop HF, et al. Natural convection of alumina-water nanofluid in an open cavity having multiple porous layers. *Int J Heat Mass Transf.* [2018](#);125:648–657.
- [10] Astanina MS, Sheremet M, Umavathi CJ. Unsteady natural convection in a partially porous cavity having a heatgenerating source using local thermal non-equilibrium model. *Int J Numer Methods Heat Fluid Flow.* [2019](#);29(6):1902–1919.
- [11] Asl AK, Hossainpour S, Rashidi M, et al. Comprehensive investigation of solid and porous fins influence on natural convection in an inclined rectangular enclosure. *Int J Heat Mass Transf.* [2019](#);133:729–744.
- [12] Sheremet MA, Pop I. Effect of local heater size and position on natural convection in a tilted nanofluid porous cavity using LTNE and Buongiorno’s models. *J Mol Liq.* [2018](#);266:19–28.
- [13] Alsabery AI, Tayebi T, Chamkha AJ, et al. Effect of rotating solid cylinder on entropy generation and convective heat transfer in a wavy porous cavity heated from below. *Int Commun Heat Mass Transfer.* [2018](#);95:197–209.
- [14] Sadeghi MS, Tayebi T, Dogonchi AS, et al. Analysis of hydrothermal characteristics of magnetic Al_2O_3 - H_2O nanofluid within a novel wavy enclosure during natural convection process considering internal heat generation. *Math Methods Appl Sci.* [2020](#).
- [15] Alsabery A, Chamkha A, Hashim I, et al. Effects of nonuniform heating and wall conduction on natural convection in a square porous cavity using LTNE model. *J Heat Transfer.* [2017](#);139:122008.
- [16] Salyan S, Suresh S. Green synthesis and characterization of hexagonal shaped MgO nanoparticles using insulin plant (*costus pictus* D. Don) leave extract and its antimicrobial as well as anticancer activity. *Adv Powder Technol.* [2018](#);29:1685–1691.

- [17] Singh SK, Sarkar J. Improving hydrothermal performance of hybrid nanofluid in double tube heat exchanger using tapered wire coil turbulator. *Adv Powder Technol.* **2020**;31(5):2092–2100.
- [18] Kumar V, Sarkar J. Experimental hydrothermal characteristics of minichannel heat sink using various types of hybrid nanofluids. *Adv Powder Technol.* **2019**;31(2):621–631.
- [19] Sivasankaran S, Alsabery A, Hashim I. Internal heat generation effect on transient natural convection in a nanofluid-saturated local thermal non-equilibrium porous inclined cavity. *Physica A.* **2018**;509:275–293.
- [20] Dogonchi AS, Chamkha AJ, Seyyedi SM, et al. Viscous dissipation impact on free convection flow of Cu-water nanofluid in a circular enclosure with porosity considering internal heat source. *J Appl Computat Mech.* **2019**;5:717–726.
- [21] Alsabery AI, Tayebi T, Chamkha AJ, et al. Re-epithelialization and immune cell behaviour in an ex vivo human skin model. *Sci Rep.* **2020**;10:1–22.
- [22] Dogonchi A, Waqas M, Ganji D. Shape effects of copper-oxide (CuO) nanoparticles to determine the heat transfer filled in a partially heated rhombus enclosure: CVFEM approach. *Int Commun Heat Mass Transfer.* **2019**;107:14–23.
- [23] Alsabery A, Chamkha A, Saleh H, et al. Natural convection flow of a nanofluid in an inclined square enclosure partially filled with a porous medium. *Sci Rep.* **2017**;7:2357.
- [24] Chamkha AJ, Ismael MA. Natural convection in differentially heated partially porous layered cavities filled with a nanofluid. *Numer Heat Transfer, Part A.* **2014**;65:1089–1113.
- [25] Sardari PT, Babaie-Mahani R, Giddings D, et al. Energy recovery from domestic radiators using a compact composite metal foam/PCM latent heat storage. *J Clean Prod.* **2020**;257:120504.
- [26] Mahdi JM, Mohammed HI, Hashim ET, et al. Solidification enhancement with multiple PCMs, cascaded metal foam and nanoparticles in the shell-and-tube energy storage system. *Appl Energy.* **2020**;257:113993.
- [27] Sardari PT, Giddings D, Grant D, et al. Discharge of a composite metal foam/phase change material to air heat exchanger for a domestic thermal storage unit. *Renewable Energy.* **2020**;148:987–1001.
- [28] Ho C, Siao C-R, Yang T-F, et al. An investigation on the thermal energy storage in an enclosure packed with micro-encapsulated phase change material. *Case Stud Therm Eng.* **2021**;25:100987.
- [29] Yan W-M, Ho C, Tseng Y-T, et al. Numerical study on convective heat transfer of nanofluid in a minichannel heat sink with micro-encapsulated PCM-cooled ceiling. *Int J Heat Mass Transf.* **2020**;153:119589.
- [30] Ho C-J, Huang J, Tsai P, et al. Water-based suspensions of Al₂O₃ nanoparticles and MEPCM particles on convection effectiveness in a circular tube. *Int J Therm Sci.* **2011**;50:736–748.
- [31] Ho C, Guo Y-W, Yang T-F, et al. Numerical study on forced convection of water-based suspensions of nanoencapsulated PCM particles/Al₂O₃ nanoparticles in a mini-channel heat sink. *Int J Heat Mass Transf.* **2020**;157:119965.
- [32] Ho C-J, Chen W-C, Yan W-M. Correlations of heat transfer effectiveness in a minichannel heat sink with water-based suspensions of Al₂O₃ nanoparticles and/or MEPCM particles. *Int J Heat Mass Transf.* **2014**;69:293–299.
- [33] Seyf HR, Zhou Z, Ma H, et al. Three dimensional numerical study of heat-transfer enhancement by nano-encapsulated phase change material slurry in microtube heat sinks with tangential impingement. *Int J Heat Mass Transf.* **2013**;56:561–573.
- [34] Reza Seyf H, Wilson MR, Zhang Y, et al. Flow and heat transfer of nanoencapsulated phase change material slurry past a unconfined square cylinder. *J Heat Transfer.* **2014**;136(5):051902.
- [35] Eisapour M, Eisapour AH, Hosseini M, et al. Exergy and energy analysis of wavy tubes photovoltaic-thermal systems using microencapsulated PCM nano-slurry coolant fluid. *Appl Energy.* **2020**;266:114849.
- [36] Ghalambaz M, Chamkha AJ, Wen D. Natural convective flow and heat transfer of Nano-Encapsulated Phase Change Materials (NEPCMs) in a cavity. *Int J Heat Mass Transf.* **2019**;138:738–749.
- [37] Hajjar A, Mehryan S, Ghalambaz M. Time periodic natural convection heat transfer in a nano-encapsulated phase-change suspension. *Int J Mech Sci.* **2020**;166:105243.

- [38] Alsedais N, Aly AM. Double-diffusive convection from an oscillating baffle embedded in an astroid-shaped cavity suspended by nano encapsulated phase change materials: ISPH simulations. *Waves Random Complex Media*. 2021; 1–20.
- [39] Raizah Z, Aly AM. Double-diffusive convection of a rotating circular cylinder in a porous cavity suspended by nano-encapsulated phase change materials. *Case Stud Therm Eng*. 2021;24:100864.
- [40] Ghalambaz M, Zadeh SMH, Mehryan S, et al. Free convection of a suspension containing nano-encapsulated phase change material in a porous cavity; local thermal non-equilibrium model. *Heliyon*. 2020;6:e03823.
- [41] Chai L, Shaukat R, Wang L, et al. A review on heat transfer and hydrodynamic characteristics of nano/microencapsulated phase change slurry (N/MPCS) in mini/microchannel heat sinks. *Appl Therm Eng*. 2018;135:334–349.
- [42] Chen B, Wang X, Zeng R, et al. An experimental study of convective heat transfer with microencapsulated phase change material suspension: laminar flow in a circular tube under constant heat flux. *Exp Therm Fluid Sci*. 2008;32:1638–1646.
- [43] Khanafer K, Vafai K. A critical synthesis of thermophysical characteristics of nanofluids. *Int J Heat Mass Transf*. 2011;54:4410–4428.
- [44] Chamkha A, Doostanidezfuli A, Izadpanahi E, et al. Phase-change heat transfer of single/hybrid nanoparticles-enhanced phase-change materials over a heated horizontal cylinder confined in a square cavity. *Adv Powder Technol*. 2017;28:385–397.
- [45] Author Biography. In: Zienkiewicz OC, Taylor RL, Nithiarasu P, editor. *The finite element method for fluid dynamics* (seventh edition). Oxford: Butterworth-Heinemann; 2014. p. ii.
- [46] Kalabin EV, Kanashina MV, Zubkov PT. Natural-convective heat transfer in a square cavity with time-varying side-wall temperature. *Numer Heat Transfer Part A*. 2005;47:621–631.
- [47] Calcagni B, Marsili F, Paroncini M. Natural convective heat transfer in square enclosures heated from below. *Appl Therm Eng*. 2005;25:2522–2531.
- [48] Baytas AC, Pop I. Free convection in a square porous cavity using a thermal nonequilibrium model. *Int J Therm Sci*. 2002;41:861–870.